# Spacecraft Component Detection in Point Clouds

Quanmao Wei[1,2], Zhiguo Jiang[1,2], Haopeng Zhang[1,2(✉)], and Shanlan Nie[1,2]

[1] School of Astronautics, Image Processing Center, Beihang University, Beijing 100191, People's Republic of China
zhanghaopeng@buaa.edu.cn
[2] Beijing Key Laboratory of Digital Media, Beijing 100191, People's Republic of China

**Abstract.** Component detection of spacecraft is significant for on-orbit operation and space situational awareness. Solar wings and main body are the major components of most spacecrafts, and can be described by geometric primitives like planes, cuboid or cylinder. Based on this prior, pipeline to automatically detect the basic components of spacecraft in 3D point clouds is presented, in which planes, cuboid and cylinder are successively detected. The planar patches are first detected as possible solar wings in point clouds of the recorded object. As for detection of the main body, inferring a cuboid main body from the detected patches is first attempted, and a further attempt to extract a cylinder main body is made if no cuboid exists. Dimensions are estimated for each component. Experiments on satellite point cloud data that are recovered by image-based reconstruction demonstrated effectiveness and accuracy of this pipeline.

**Keywords:** Component detection · Structure analysis · Spacecraft Point clouds

## 1 Introduction

Three dimensional (3D) models, compared to two dimensional (2D) images, are free of perspective projection and can represent the spatial characters of objects, e.g. position, orientation, dimensions and shape. 3D models of space objects have enormous potential for aids in advanced space missions such as autonomous rendezvous, docking and on-orbit self-serving [1,9,10,13]. And detection of specific components, such as solar wings and main body, is a critical task. However, the raw and unstructured point cloud data, which could be acquired by laser scanning [1] or recovered from multi-view images [19], is still primary and can not directly represent the structural information of the recorded object. Addressing on this problem, this paper proposes an automatic pipeline to detect the basic components of spacecrafts, i.e. solar wings and main body.

Recent advances made in 3D acquisition technologies result in a broad availability of 3D models and point clouds, and it further facilitates development of


Y. Wang et al. (Eds.): IGTA 2017, CCIS 757, pp. 210–218, 2018.
https://doi.org/10.1007/978-981-10-7389-2_21

approaches to process and analyze these data [2,6]. For most of these approaches, detection of geometric primitives in the scene is a crucial procedure [8,15]. To construct 3D building models, plane detection is generally employed for rooftop segmentation [3,14], and to model installations in industrial sites, cylinders, which are frequently encountered in industrial scenes, are detected as description of pipes or part of other complex installations [11,12]. As for spacecrafts, most of their solar wings and main bodies can be described as specific geometric shape like plane, cuboid and cylinder. Therefore, higher-level structural representations could be generated by detection of such geometric primitives.

In our proposed pipeline, planar primitives are first detected by Hough transform (HT) paradigm [4,7], and subsequently updated to planar patches which are treated as possible solar wings. Next, through checking pair-wise geometry relations among these detected patches, existence of cuboid main body is identified. Then the cuboid main body is further estimated with the patches (faces) belong to it if there exists one, otherwise, the detection of cylinder main body is performed in the residual points. Simultaneously, dimension information is estimated for each detected component. Experiments are conducted on point cloud data of satellites that are recovered by image-based method [5,16,17,19]. The results of detection and dimension estimation demonstrate the effectiveness and accuracy of the proposed pipeline.

The rest of this paper is organized as follow. Section 2 gives a detailed description of the proposed pipeline of successive detections for planes, cuboid and cylinder, along with the dimension estimation. Experiment results of the proposed pipeline is presented and analyzed in Sect. 3. A final conclusion of this paper is presented in Sect. 4.

## 2 Detection Pipeline

The block diagram of the proposed pipeline is shown in Fig. 1. It consists of four stages of processing, namely preprocessing, successive detections of possible solar wings, cuboid main body and cylinder main body. All the four stages are respectively explained as follow.

### 2.1 Preprocessing

The point cloud data used in our cases are generated by reconstruction from images. These data, compared to laser scanning data, contain severe noise and outliers. Statistical analysis of the k nearest neighbor (knn) can effectively identify outliers that are randomly distributed. However, outliers can be also more structured, as shown in Fig. 3(a), outliers in form of high-density clusters exist separating from the object points. To remove such outliers, clustering method implemented by region growing is used. The input point clouds is clustered into groups by region growing, and only the biggest group is regarded as set of object points.

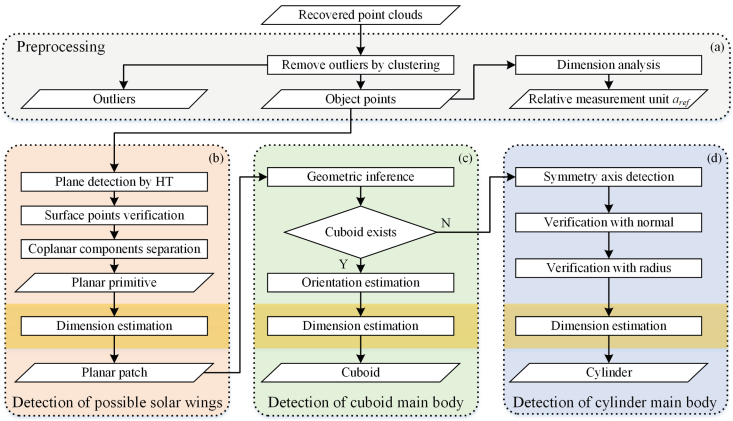


**Fig. 1.** Block diagram showing the proposed pipeline. (a) Preprocessing; (b) detection of possible solar wings; (c) detection of cuboid main body; and (d) detection of cylinder main body.

Furthermore, to handle the scale variation in different point cloud data, a relative dimensional unit $a_{ref}$ is adaptively defined. In our experiments $a_{ref}$ is set as $kD_3$, where $D_3$ is the dimension along the last eigenvector ($\lambda_1 \geq \lambda_2 \geq \lambda_3$) of the covariance tensor of the object points. To keep a balance between the precision and efficiency, $k$ is set to 0.01.

## 2.2 Detection of Solar Wings

In our plane detection approach, a 3D plane $\Pi$ is formulated as $s_x X + s_y Y + s_z Z + s_d = 0$, and three separate Hough detections are performed in parallel. For each Hough detection, to uniquely define the plane, one parameter among $s_x$, $s_y$ and $s_z$ is fixed to 1 and the other two parameters are discretized in range $[-1, 1]$. $\Pi$ is finally defined as the plane that has the most points among the three separate detection results. In this way, planes with all possible orientations are considered, and trade-off between the accuracy and computation consumption can be easily adjusted too. Besides, only neighborhood of the normal vector need to be voted for each point, when putting the noisy normal information into detection, it accelerates the computation a lot.

Surface points, which belong to the detected plane, are then verified by distance proximity and orientation proximity. However, these points may belong to multiple coplanar solar wings and part of component surfaces that intersect the determined solar wing. To separate these points, a distance proximity based region growing approach is utilized. The group that has the maximum size is kept and finally accepted as possible solar wing if its size is big enough.

Since a solar wing is a bounded planar patch rather than a infinitely extended plane, we update the detected plane primitive to a patch in the dimension estimation step. First the surface points are fitted by the least squares method and

all these surface points are projected to the fitted plane. Then two edge directions $u$, $v$, as well as the dimensions along these edge directions, are estimated by finding the minimum bounding rectangle (MBR) of the projected points.

Multiple patches are iteratively detected, until no point is residual or the current detected patch is too small. Before inferring the cuboid faces, all these detected patches are treated as possible solar wings.

### 2.3 Detection of Cuboid Main Body

Faces of the cuboid main body, if exist, may also be detected as patches, as shown in Fig. 3(c-1). An inferring approach is proposed to distinguish these patches. As for a cuboid, there are two kinds of pair-wise geometry relations among its 6 faces, the opposite faces and the adjacent faces. To identify the existence of such cuboid, criteria to verify there relations are exploited.

1. **Criterion for two opposite faces**: (a) their plane normals are parallel and edges of them are respectively parallel too; (b) the line passing their centers is parallel to the plane normal.
2. **Criterion for two adjacent faces**: (a) their plane normals are perpendicular and edges of them are respectively parallel or perpendicular; and (b) they have one common edge.

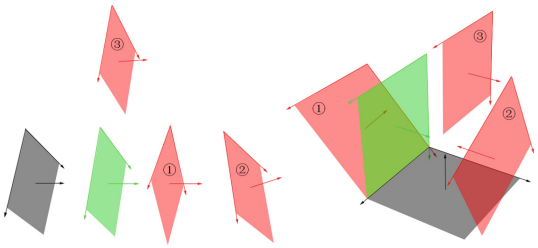


**Fig. 2.** Criteria for opposite (left) and adjacent (right) faces. The gray patch is a reference patch, the green one passes all the criteria, while the red ones do not satisfy the orientation (case 1 and 2) or position (case 3) requirements. (Color figure online)

For criteria of both opposite and adjacent faces, condition (a) constrains the orientation relations so that case 1 and case 2 in Fig. 2 can be filtered, condition (b) constrains the position relations so that case 3 in Fig. 2 can be filtered. A group of cuboid faces, among which each pair of patches satisfy the opposite or adjacent criterion, can be extracted if there exists a cuboid. Then orientation and dimensions of this cuboid is further estimated as follow.

First, the edge confidence coefficient is estimated. For one edge $E$ of some patch $\Pi_q$, all the surface points are projected to $E$, and the distribution range of

the projected points along $E$ is split into $N_{Bin}$ ($N_{Bin} = 10$ in our experiments) bins. The confidence associated with $E$ is then estimated as

$$conf = \frac{-\Sigma_{i=1}^{N_{Bin}}(p_i \ln p_i)}{\ln N_{Bin}} \tag{1}$$

Where $p_i = n_i/N_{Pts}$, $n_i$ is the number of points that fall in the i-th bin, $N_{Pts}$ is the total number of surface points of $\Pi_q$. $En = -\Sigma_{i=1}^{N_{Bin}}(p_i \ln p_i)$ represents the distribution entropy, and $En_{Max} = \ln N_{Bin}$ is the maximum value that $En$ can reach when these points are uniformly distributed.

Then, three orthogonal directions are estimated to define the orientation. Each patch has three orthogonal direction vectors, i.e. one plane normal and two edge vectors. The plane normal is preferred as it is generally more accurate and credible than the edge ones. For a face direction $n^f$ of the cuboid, assume there are $N_n$ ($N_n \leq 2$) plane normals $n_i^n$, $i = 0, 1, ..., N_n$, and $N_e$ ($N_e \leq 4$) edge directions $n_j^e$, $j = 0, 1, ..., N_e$, that are associated with $n^f$. Then $n^f$ is estimated as

$$\hat{n^f} = \begin{cases} \frac{e_2^2 n_1^n + e_1^2 n_2^n}{e_1^2 + e_2^2} & N_n = 2, \\ n_1^n & N_n = 1, \\ \frac{\Sigma_{j=1}^{N_e} conf_j^2 n_j^e}{\Sigma_{j=1}^{N_e} conf_j^2} & N_n = 0. \end{cases} \tag{2}$$

Where $e$ is the fitted error of the surface plane, $conf_i$ is the confidence associated with $n_i^e$. To guarantee the orthogonality of the estimated face directions, the diagonal matrix of SVD of the direction matrix is set to identity.

The dimensions of the cuboid is finally estimated. For each patch, it can offer 2.5 size information, i.e. two edge lengths and an intercept along the face vector. The intercept is also preferred to be used. For the face direction $\hat{n^f}$, assume the projections of center of the $N_n$ perpendicular planes are $l_i^n$, $i = 1, 2, ..., N_n$, and projections of center of the $N_e$ perpendicular edge pairs are $a_j^e$ and $b_j^e$, $j = 1, 2, ..., N_e$, then the dimension along $\hat{n^f}$ is estimated as

$$D_{\hat{n^f}} = \begin{cases} abs(l_1^n - l_2^n) & N_n = 2, \\ \max\limits_{q=a,b}\{abs(l_1^n - med(q_j^e))\} & N_n = 1, \\ abs(med(a_j^e) - med(b_j^e)) & N_n = 0. \end{cases} \tag{3}$$

Note that, due to the noise and detail of the cuboid main body, a face might be detected as multiple patches. To handle these cases, patches that are close to a face of the detected cuboid and can be mostly included by that face will be merged into the cuboid.

### 2.4 Detection of Cylinder Main Body

If no cuboid main body is detected in Sect. 2.3, a subsequent attempt will be made to detect a cylinder one, on the assumption that there is at least one cuboid or cylinder main body in one spacecraft.

Based on the observation that the surface normals would always intersect with the symmetry axis, an axial-symmetry-based method to detect cylinder is proposed. First, normal of each point is drawn in a discretized 3D space, points (voxels) at which more than 5 normals intersect are then used to estimate the symmetry axis by PCA. The axis is defined as the line that is parallel to the first eigenvector and passes the mean location of these intersections.

To verify the surface points of the determined cylinder, normal vector and radius are successively used. A point is initially accepted as a surface point if the vertical distance of its normal to the symmetry axis is small. Then a mean radius $R$ is evaluated with these verified points. And for each verified points, it is re-verified with the radius information. Only points located around the cylinder faces with radius $R$ are final accepted. $R$ is updated at last, and the length of the cylinder is defined as the dimension of the surface points along the axis.

## 3 Experiment

Point cloud data used in our experiments are recovered from simulated images sequences [18,19]. The objects recorded in these data are Helios-2A (1st row in Fig. 3) and Tiangong-1 (2nd row in Fig. 3). Thresholds and parameter values used in our experiments, which have been obtained by trial and error experiments, can be found in Table 1.

**Table 1.** Parameters for detections in the proposed pipeline

| Parameters | Value |
|---|---|
| Discretization accuracy for $s_x$, $s_y$ and $s_z$ | 0.01 |
| Discretization accuracy for $s_d$ | $1 \times a_{ref}$ |
| Distance threshold in planar surface points verification ($T_{dis}$) | $(2-4) \times a_{ref}$ |
| Angle threshold in planar surface points verification ($T_{ang}$) | 15° |
| Angle deviation for parallel and perpendicular patches | 5° |
| Distance deviation for adjacent planes | $5 \times a_{ref}$ |

The component detection results of Helios-2A and Tiangong-1 are illustrated in Fig. 3. Note that the main body detection result of Helios-2A do not include the loads below, which complicate the shape of main body. And the main body of Tiangong-1 is treated as a whole cylinder while it actually contains two capsules. Our pipeline effectively detect the solar wings and main bodies except for solar wing of Helios-2A. Due to the lack of texture, the solar wing of Helios-2A is few recovered except for its frame, and our pipeline failed to detect plane in such sparse points.

To quantitatively evaluate the accuracy of the detection results, the relative dimension ratio ($Ratio_{Est}$) of each detected component is computed, along with

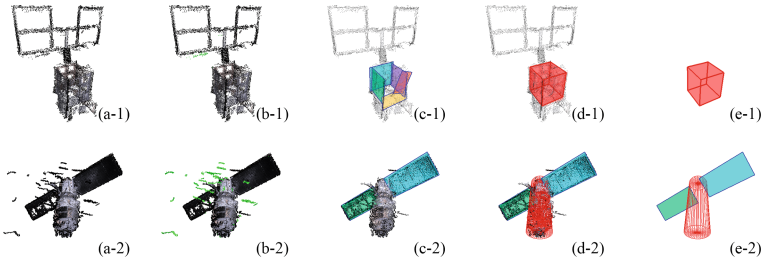


**Fig. 3.** Results of component detection. (a) Input point clouds that contain severe noise and high-density clustering outliers. (b) Outliers (in green) are effectively identified. (c) Planes are detected and updated to planar patches. (d) Infer a cuboid main body from the patches or detect a cylinder one from the residual points. (e) A clear view of the detected components. (Color figure online)

its ground truth ($Ratio_{GT}$), which is directly measured from the models. The comparison is presented in Table 2, dimension ratios of solar wing and cuboid main body are in form that $l1 : l2 : l3$ ($l1 \leq l2 \leq l3$), and dimension ratio of a cylinder is ratio of its length to its radius. The deviations are all less than 20%.

**Table 2.** Relative dimension ratio of each component

| Object | Component | $Ratio_{GT}$ | $Ratio_{Est}$ | Deviation (%) |
|---|---|---|---|---|
| Helios-2A | Cuboid MB | 1 : 1 : 1.25 | 1 : 1.00 : 1.17 | 0.03, 6.4 |
| | Solar wing | 1 : 2.43 | Undetected | – |
| Tiangong-1 | Cylinder MB | 1 : 5.94 | 1 : 6.09 | 2.5 |
| | Solar wing | 1 : 2.54 | 1 : 2.08 | 18.1 |
| | | | 1 : 2.24 | 11.8 |

## 4 Conclusion

In this paper, a pipeline is proposed to automatically detect the basic components of spacecrafts, which results in a higher structural level representations. The basic components are treated as geometric primitives such as planes, cuboid or cylinder. Therefore, detections for such primitives are successively conducted. To detect the cuboid, an approach to infer a cuboid from group of patches is proposed. Specifically, criteria to determine cuboid faces are proposed, as well as methods to estimate the orientation and dimensions of the cuboid. And a novel axial-symmetry-based cylinder detection approach is also presented, in which the cylinder is robustly detected through detection of its axis and verification of its surface points. The experiment performance on the recovered point cloud data, which are relative sparse and inhomogeneous on the one hand, and surfer from severe noise and outliers on the other hand, verified the effectiveness and accuracy.

To further improve this pipeline, more structure details, such as antennas, imaging sensors and supporting structure, should be considered in, as well as shape refinement of the detected components. Global structure properties of the object and relations of different components could be further exploited to improve the accuracy.

**Acknowledgements.** This work was supported in part by the National Natural Science Foundation of China (Grant Nos. 61501009, 61371134 and 61071137), the National Key Research and Development Program of China (2016YFB0501300, 2016YFB0501302), the Aerospace Science and Technology Innovation Fund of CASC, and the Fundamental Research Funds for the Central Universities.

## References

1. Benninghoff, H., Boge, T., Rems, F.: Autonomous navigation for on-orbit servicing. KI-Knstliche Intell. **28**(2), 77–83 (2014)
2. Berger, M., Tagliasacchi, A., Seversky, L.M., Alliez, P., Guennebaud, G., Levine, J.A., Sharf, A., Silva, C.T.: A survey of surface reconstruction from point clouds. Comput. Graph. Forum **36**, 301–329 (2016). Wiley Online Library
3. Cao, R., Zhang, Y., Liu, X., Zhao, Z.: Roof plane extraction from airborne lidar point clouds. Int. J. Remote Sens. **38**(12), 3684–3703 (2017)
4. Duda, R.O., Hart, P.E.: Use of the Hough transformation to detect lines and curves in pictures. Commun. ACM **15**(1), 11–15 (1972)
5. Furukawa, Y., Ponce, J.: Accurate, dense, and robust multi-view stereopsis. In: 2007 IEEE Conference on Computer Vision and Pattern Recognition, pp. 1–8 (2007)
6. Grilli, E., Menna, F., Remondino, F.: A review of point clouds segmentation and classification algorithms. Int. Arch. Photogramm. Remote Sens. Spatial Inf. Sci. **XLII–2/W3**, 339–344 (2017)
7. Hough, P.: Method and means for recognizing complex patterns (1962)
8. Limberger, F.A., Oliveira, M.M.: Real-time detection of planar regions in unorganized point clouds. Pattern Recogn. **48**(6), 2043–2053 (2015)
9. Opromolla, R., Fasano, G., Rufino, G., Grassi, M.: Pose estimation for spacecraft relative navigation using model-based algorithms. IEEE Trans. Aerosp. Electron. Syst. **53**(1), 431–447 (2017)
10. Ouyang, B., Yu, Q., Xiao, J., Yu, S.: Dynamic pose estimation based on 3D point clouds. In: 2015 IEEE International Conference on Information and Automation, pp. 2116–2120. IEEE (2015)
11. Pang, G., Qiu, R., Huang, J., You, S., Neumann, U.: Automatic 3D industrial point cloud modeling and recognition. In: 2015 14th IAPR International Conference on Machine Vision Applications (MVA), pp. 22–25. IEEE (2015)
12. Rabbani, T., Van Den Heuvel, F.: Efficient Hough transform for automatic detection of cylinders in point clouds. In: ISPRS WG III/3, III/4, vol. 3, pp. 60–65 (2005)
13. Ruel, S., Luu, T., Berube, A.: Space shuttle testing of the tridar 3D rendezvous and docking sensor. J. Field Rob. **29**(4), 535–553 (2012)
14. Tarsha-Kurdi, F., Landes, T., Grussenmeyer, P.: Hough-transform and extended ransac algorithms for automatic detection of 3D building roof planes from lidar data. In: Proceedings of the ISPRS Workshop on Laser Scanning, vol. 36, pp. 407–412 (2007)

15. Vosselman, G., Gorte, B.G., Sithole, G., Rabbani, T.: Recognising structure in laser scanner point clouds. Int. Arch. Photogramm. Remote Sens. Spat. Inf. Sci. **46**(8), 33–38 (2004)
16. Wu, C.: Towards linear-time incremental structure from motion. In: 2013 International Conference on 3D Vision - 3DV 2013, pp. 127–134 (2013)
17. Wu, C., Agarwal, S., Curless, B., Seitz, S.M.: Multicore bundle adjustment. In: CVPR 2011, pp. 3057–3064 (2011)
18. Zhang, H., Liu, Z., Jiang, Z., An, M., Zhao, D.: BUAA-SID1. 0 space object image dataset. Spacecr. Recovery Remote Sens. **31**(4), 65–71 (2010)
19. Zhang, H., Wei, Q., Jiang, Z.: Sequential-image-based space object 3D reconstruction. J. Beijing Univ. Aeronaut. Astronaut. **42**(2), 273–279 (2016)